Structural and magnetic properties of Ni1−xZnxFe2O4 (x=0, 0.5 and 1) nanopowders prepared by sol–gel method

ARTICLE · DECEMBER 2013

DOI: 10.1016/j.jmmm.2013.07.060

Journal of Magnetism and Magnetic Materials 348 (2013) 44–50

Contents lists available at ScienceDirect

Journal of Magnetism and Magnetic Materials

journal homepage: www.elsevier.com/locate/jmmm

Structural and magnetic properties of $Ni_{1-x}Zn_xFe_2O_4$ ($x=0$, 0.5 and 1) nanopowders prepared by sol–gel method

Pengzhao Gao [a,b], Xia Hua [a], Volkan Degirmenci [a], David Rooney [a], Majeda Khraisheh [c], Robert Pollard [d], Robert M. Bowman [d], Evgeny V. Rebrov [a,*]

[a] School of Chemistry and Chemical Engineering, Queen's University Belfast, Stranmillis Road, Belfast BT9 5AG, UK
[b] College of Materials Science and Engineering, Human University, Changsha 410082, China
[c] Department of Chemical Engineering, Qatar University, Doha, Qatar
[d] Centre for Nanostructured Media, School of Mathematics & Physics, Queen's University Belfast, Belfast BT7 1NN, UK

ARTICLE INFO

Article history:
Received 29 May 2013
Received in revised form
23 July 2013
Available online 6 August 2013

Keywords:
Sol–gel method
Ferrite
Magnetization
Radiofrequency heating

ABSTRACT

A series of nanostructured Ni–Zn ferrites $Ni_{1-x}Zn_xFe_2O_4$ ($x=0$, 0.5 and 1) with a grain size from 24 to 65 nm have been prepared with a sol–gel method. The effect of composition and sintering temperature on morphology, magnetic properties, Curie temperature, specific heating rate at 295 kHz and hysteresis loss have been studied. The highest coercivity of 50 and 40 Oe, were obtained for $NiFe_2O_4$ and $Ni_{0.5}Zn_{0.5}Fe_2O_4$ samples with the grain size of 35 and 29 nm, respectively. The coercivity of Ni and Ni–Zn mixed ferrites decreased with temperature. The Bloch exponent was 1.5 for all samples. As the grain size increased, the Curie temperature of $NiFe_2O_4$ increased from 849 to 859 K. The highest saturation magnetization of 70 emu/g at 298 K and the highest specific heating rate of 1.6 K/s under radiofrequency heating at 295 kHz were observed over $NiFe_2O_4$ calcined at 1073 K. Both the magnitude of the hysteresis loss and the temperature dependence of the loss are influenced by the sintering temperature and composition.

1. Introduction

Nanostructured spinel type ferrites are promising materials that could be used as susceptors of induction heating in catalytic chemical reactors due to their high Curie temperatures and moderate magnetic losses in the kHz range. Moreover, they can be employed as magnetic catalysts or catalyst carriers which facilitate separation [1]. The use of nanostructured magnetic materials for radiofrequency heating (RF) and magnetic separation within a chemical reactor system provides a novel process intensified platform for system integration [2]. In these applications, magnetic nanoparticles embedded into composite catalytic microparticles are used as susceptors of induction or microwave heating [3,4]. RF heating provides efficient, fast and uniform heat transfer into catalyst [5,6] and flowing fluid [7,8].

Spinel ferrites have the general molecular formula $(A^{2+})[B_2{}^{3+}]O_4{}^{2-}$ where A^{2+} and B^{3+} are the divalent and trivalent cations occupying tetrahedral (A) and octahedral (B) interstitial positions of the fcc lattice formed by $O_2{}^{2-}$ ions. The Néel (Curie) temperature and magnetic properties of ferrite materials depend on the type of cations and their distribution among the two interstitial positions, which in turn depends on the method of synthesis, sintering conditions and the grain size [9,10]. As the grain size of nanostructured ferrites is much smaller than the skin depth, their heating rate within kHz range is considerably higher than that of the bulk ferrites. The heating rates can further be adjusted by changing chemical composition of magnetic nanoparticles and their synthesis conditions.

Nanocrystalline Ni ferrites have been synthesized via co-precipitation [11], sol–gel [12], microwave [13], ball milling [14], and aerosolization [15]. Sol–gel is a flexible technique to fluctuate the properties of the material by optimizing the different parameters such as gelation time, temperature, reagent's concentration and pH of the medium. The advantages of the sol–gel process include high purity of the resulting materials, their chemical homogeneity, and high degree of control over particle and grain size. Furthermore, the method can be easily scaled up to a large production scale which is crucial for the development of chemical processes involving RF heating.

Nanostructured nickel ferrite is a mixed spinel [9]. It exhibits noncollinear spin structure and the magnetic moment is appreciably lower than that for the bulk material. The mean grain size is typically in the 20–50 nm range and it gradually increases with increasing sintering temperature [16]. The effect of increasing the sintering temperature could also change the microstructure of the materials which, in turn, affects magnetic properties of the

* Corresponding author. Tel.: +44 2890974627.
E-mail addresses: e.rebrov@qub.ac.uk, e.rebrov73@gmail.com (E.V. Rebrov).

0304-8853/$ - see front matter Crown Copyright © 2013 Published by Elsevier B.V. All rights reserved.
http://dx.doi.org/10.1016/j.jmmm.2013.07.060

materials [10,17]. The high temperature treatment severely reduces the specific surface area of the resulting materials so that they could not be formed in a desired shape, i.e. pelleted. An addition of 1–3 wt% $5PbO \cdot SiO_2$ or $5PbO \cdot B_2O_3$ powders was reported to be an effective method to decrease the sintering temperature and to obstruct the movement of grain boundaries which facilitates minimizing the ferrite grain size in $Ni_{1-x}Zn_xFe_2O_4$ composite materials [18]. Preparation of ferrite/SiO_2 composites containing 5–30 wt% nanostructured ferrite is another way to reduce the sintering temperature [19]. However, the saturation magnetization and the specific heating rate in the RF range of such composite materials are substantially reduced as compared to that of pure ferrites. Besides, the formation of microcracks in composite materials during high temperature sintering is another problem.

The sintering temperature required for the formation of a single phase ferrite can also be reduced by Zn addition [20]. It was reported that $Ni_{0.65}Zn_{0.35}Fe_2O_4$ obtained by the sol–gel method has a high saturation magnetization of 80 emu/g even when sintered at 1373 K [21]. Higher Néel (Curie) temperatures and mechanical hardness have also been reported for $Ni_{0.3}Zn_{0.7}Fe_2O_4$ obtained through the sol–gel route [22]. However temperatures in excess of 1123 K are not desirable in large scale synthesis of ferrite materials as operational costs would increase considerably.

Single phase nanosized $Ni_{1-x}Zn_xFe_2O_4$ materials can be formed after sintering above 873 K [11]. $ZnFe_2O_4$ is a normal spinel with Zn^{2+} ions located in A-positions and Fe^{3+} ions in B-positions. It is paramagnetic at room temperature. However under specific synthesis conditions, such as mechanochemical activation [23,24] and aerogel procedure [25], a nanocrystalline $ZnFe_2O_4$ spinel can be obtained where some Fe^{3+} ions occupy tetrahedral, as well as octahedral sites forming a mixed or inverse spinel structure [23,26]. The strong superexchange interaction among these sites results in an unusually high magnetization as compared to normal spinels. It is well established that for $Ni_{1-x}Zn_xFe_2O_4$ with x less than 0.5, the Fe moments at A and B sites have collinear arrangements and with x greater than 0.5, have noncollinear arrangements [27]. Therefore, it is essential to study the magnetic properties of $Ni_{1-x}Zn_xFe_2O_4$ materials with $x=0.0$, 0.5 and 1.0.

Lowering of the sintering temperature is a primary objective of this study to reduce energy consumption. The paper further focuses on optimization of the method for preparation of $Ni_{1-x}Zn_xFe_2O_4$ ferrites and the study of physicochemical and magnetic properties and specific heating rates of the resulting materials in the kHz range.

2. Experimental

2.1. Synthesis of materials

Nanosized $Ni_{1-x}Zn_xFe_2O_4$ materials were prepared by the citrate precursor method [28]. Iron (III) nitrate nonahydrate, nickel nitrate hexahydrate, zinc nitrate hexahydrate, citric acid, ethanol, and ammonia solution (Sigma-Aldrich, ACS grade) were used for the preparation of the starting sol. First the metal nitrates were dissolved in ethanol in required molar ratios. Citric acid was dissolved in ethanol in a separate vessel. Then the acid solution was added into the nitrate solution and stirred for 4 h. The pH of the solution was adjusted to 2. The resulting sol was stirred rigorously for 24 h then dried in an oven at 353 K to get a dry gel. The dry gel was milled and calcined in a tubular furnace in an air flow of 50 mL/min with a heating rate of 10 K/min from room temperature to 873, 973, 1073 and 1173 K to produce the corresponding ferrites. The heating rate was 2 K/min from 298 to 673 K and 5 K/min from 673 K to the final temperature. The materials were sintered for 1 h at the final temperature. The materials of $NiFe_2O_4$, $ZnFe_2O_4$ and $Ni_{0.5}Zn_{0.5}Fe_2O_4$ are labeled as Ni-FER-ST, Zn-FER-ST, Ni–Zn-FER-ST, respectively, where index ST designates their sintering temperature in K.

2.2. Characterization

The phase composition was determined using an X-ray diffractometer (X'Pert PRO) with Cu Kα radiation produced at 40 kV. The spectra were recorded at a scanning rate of 0.3° 2θ/min. The mean crystal size was obtained from the (311) peak by using the Scherrer equation [29]. The microstructure analysis was performed with a transmission electron microscope (TEM, Philips, Tecnai F20) operated at 200 kV. The nitrogen adsorption/desorption experiments were performed at 77 K with a Quantachrome NOVA 1000E nitrogen adsorption apparatus. The nonsintered dry gels (20 mg) were characterized by thermogravimetric analysis (TGA) with a STAR thermal analyzer (Mettler Toledo). The analysis was performed by heating from 293 to 1073 K with a heating rate of 10 K/min.

The magnetization curves of the materials were measured by a vibrating sample magnetometer (VSM) equipped with a 1.8 T electromagnet (Princeton Measurements Corporation MicroMag 3900) at temperatures from 298 to 823 K. The saturation magnetization (M_s), remanent magnetization (M_r) and coercivity (H_c) of the materials were determined from the magnetization curves.

The specific heating rates of ferrite powders were measured in a quartz tube (i.d.=3 mm) inserted along the center axis in an 50 mm long RF coil connected to an RF system operated at a current of 200 A and a frequency of 295 kHz (Easy Heat, Ambrell). Prior to the measurements, slurry of the materials (10 mg) in deionized water (0.08 mg) was prepared. Afterwards, the temperature of the medium was monitored with a fiber optic sensor. The specific heating rate was calculated by considering the specific heat capacities of the slurry and the ferrite.

3. Results and discussion

3.1. Optimization of sintering protocol

TGA curves during decomposition of the Ni–Zn dry gels are shown in Fig. 1. The process consists of several steps. At first, adsorbed water is removed from the $(N_2H_5)_3Ni_{1-x}Zn_xFe_2(N_2H_3COO)_9 \cdot 3H_2O$ precursor below 438 K. This corresponds to 5.0 wt% of the total weight loss, which is in agreement with the theoretical value (5.4 wt%). The second stage at 438–493 K is related to a

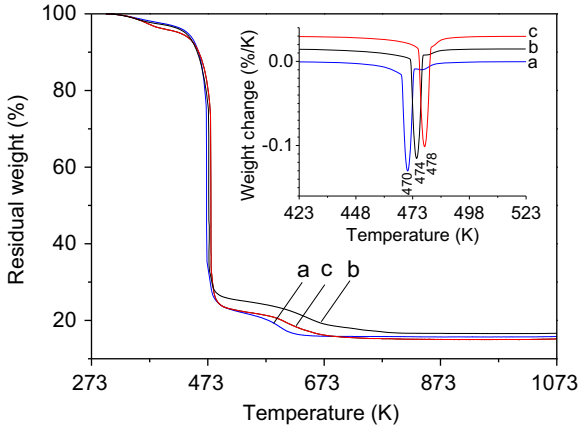

Fig. 1. Thermal gravimetrical (TG) analysis of dry gels. (a) $NiFe_2O_4$, (b) $ZnFe_2O_4$, and (c) $Ni_{0.5}Zn_{0.5}Fe_2O_4$. The corresponding differential curves (DTG) are shown in the inset.

partial decomposition of the citrate precursor. This corresponds to 70 wt% of the total weight loss. Above 493 K, the weight loss of 12 wt% corresponds to the decomposition of residual amounts of the citrate precursor and oxidation of small amounts of carbon formed during the second stage. These findings are in agreement with previous results indicating that Zn addition reduces temperature of decomposition of the citrate precursor [28]. The overall weight loss of 82.8 wt% is close to the theoretical value. The difference of 3 wt% is due to a slight deviation in ferrite stoichiometry from the nominal composition. While the corresponding spinel was the main phase, impurities of the cubic Fe_2O_3 phase (less than 5 wt%) were also observed in the XRD spectra (Fig. 2).

3.2. Effect of grain size on magnetic properties of ferrites

The physical and magnetic properties of $NiFe_2O_4$ nanopowders sintered at 873, 973, 1073, and 1173 K are listed in Table 1. The grain size of $NiFe_2O_4$ after sintering at different temperatures was determined from XRD spectra (Fig. 2). All the peaks are indexed with the standard pattern reported in JCPDF cards (#74–2081 for $NiFe_2O_4$). The Ni-FER-873 shows a sharp diffraction peak at 36° 2θ which is ascribed to the (311) plane of $NiFe_2O_4$. However other $NiFe_2O_4$ peaks are rather wide which indicates that the material has low degree of crystallinity. The $NiFe_2O_4$ spinel is the main phase in the 973–1173 K range. As the temperature increases, the grain size increases from 24 to 65 nm while the specific surface area decreases from 32.3 to 17.2 m^2/g due to aggregation of small crystallites into larger particles. The latter can also be seen in TEM images as shown in Fig. 3. The specific surface area of samples

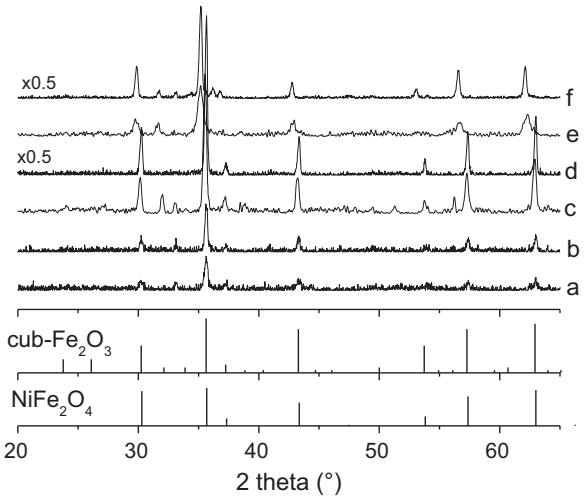

Fig. 2. XRD patterns of (a) Ni-FER-873, (b) Ni-FER-973, (c) Ni-FER-1073, (d) Ni-FER-1173, (e) Zn-FER-1073, and (f) Ni–Zn-FER-1073.

Table 1
Physical and magnetic properties of Ni-FER, Zn-FER and Ni–Zn-FER nanopowders.

Sample	Mean crystal size (nm)	Specific surface area (m^2/g)	Curie temperature (K)	Specific heating rate (K/s)
Ni-FER-873	24.2	32.3	849	0.40
Ni-FER-973	27.5	25.8	851	1.10
Ni-FER-1073	35.1	20.1	854	1.60
Ni-FER-1173	65.0	17.2	859	1.50
Ni–Zn-FER-1073	28.5	35.2	558	1.40
Zn-FER-1073	40.3	48.9	710	0.01

obtained in the present study is lower as compared to those (50–75 m^2/g) reported for sol–gel nickel ferrites sintered between 973 and 1173 K [12]. It appears that sintering at 873 K leads to a partially amorphous structure with a relatively small number of individual crystals. As the temperature increases, the relative amount of the amorphous phase decreases followed by the increase in particle size. TEM images show that the particles consist of irregular polyhedrons with necks. It could be due to the fact that magnetic attraction of tiny particles with large specific area leads to their agglomeration. The initial crystal contact points grow and form necks during sintering. The resulting particles have irregular polyhedron shape with a large particle size distribution of 50–120 nm. The sample sintered at 1173 K exhibited well defined grain boundaries, having an average grain size of 100 nm. It is important to point out that this size is much larger as compared to that obtained from the XRD measurements, which also confirms the fact that individual particles consists of several diffraction domains.

Room temperature hysteresis loops for the samples sintered at different temperatures are shown in Fig. 4. For all compositions magnetization is unsaturated up to a field of 5 kOe. Saturation magnetization (M_s) is influenced by intrinsic factors such as preferential site occupancy of the cations, composition and is also influenced by extrinsic factors like microstructure and bulk density of the ferrites [30]. It is observed that M_s is increasing with sintering temperature up to 1173 K with maximum value of M_s is 70.0 emu/g (Fig. 5).

The increased magnetization with sintering temperature is attributed to larger grain size. The maximum value is also larger than that for the bulk Ni ferrite (56 emu/g) [11]. The observed higher value of saturation magnetization could be explained on the basis of grain size and the exchange interaction among the adjacent nanometer sized grains. The exchange interaction increases M_s in a material with densely packed grains [31].

As the temperature increases, the saturation magnetization of $NiFe_2O_4$ materials decreases (Fig. 5). The variation of saturation magnetization M_s as a function of temperature can be described by the following equation [32]:

$$M_s = M_{s0}\left(1 - BT^b\right) \tag{1}$$

where B is the Bloch constant, M_{s0} is the saturation magnetization at T=0 K, and b is the Bloch exponent. Both the values have been obtained by fitting experimental data using Eq. (1) and they are listed in Table 2.

For nanostructured materials, Mills and Maradudin reported the Bloch exponent of 3/2, as for bulk materials [33]. However they found out that the Bloch constant is a function of nanoparticle size and it can be higher by a factor of 2 as compared to that of the corresponding bulk material. Theoretical work has shown that the Bloch exponent b should increase as the particle size is reduced [34]. Zhang et al. reported, b in the range 1.5–2.0 for $MnFe_2O_4$ nanoparticles with sizes in the range 5–15 nm [35]. Our results show that the Bloch constant of $NiFe_2O_4$ materials does not depend on the particle size.

The change of average crystallite size influenced the coercivity (H_c) of the ferrite samples as it was shown in a previous study [3]. Isolated nanoparticles above the onset of superparamagnetism are magnetically hard, i.e., they have a large coercivity. In contrast, nanostructured magnets consisting of densely packed grains are magnetically soft as a result of the interaction between the grains. In the Ni ferrite samples, coercivity decreases with the increase in particle size as the samples have a multidomain structure. The critical diameter (d_{cr}) was estimated by the following equation [36]:

$$d_{cr} = \frac{9\varepsilon_p}{2\pi M_{sp}^2} \tag{2}$$

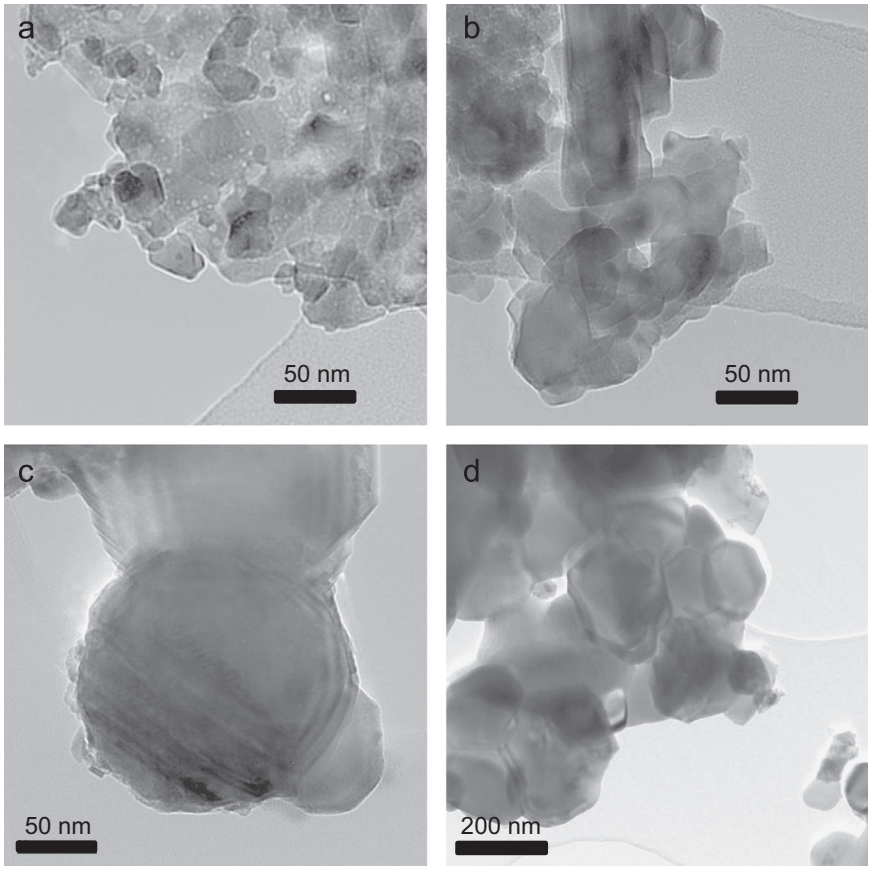

Fig. 3. TEM images of (a) Ni-FER-873, (b) Ni-FER-973, (c) Ni-FER-1073, and (d) Ni-FER-1173.

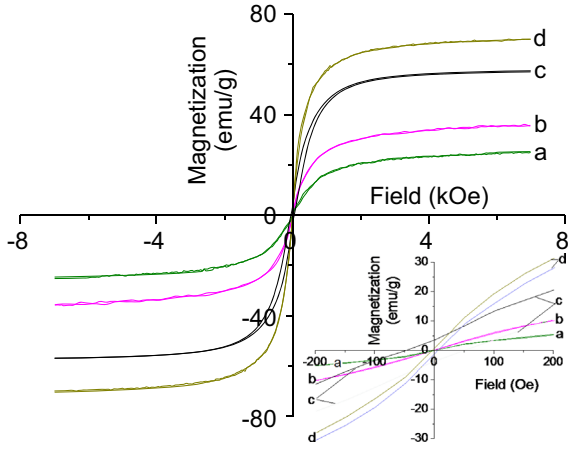

Fig. 4. Room temperature hysteresis loops. (a) Ni-FER-873, (b) Ni-FER-973, (c) Ni-FER-1073, and (d) Ni-FER-1173.

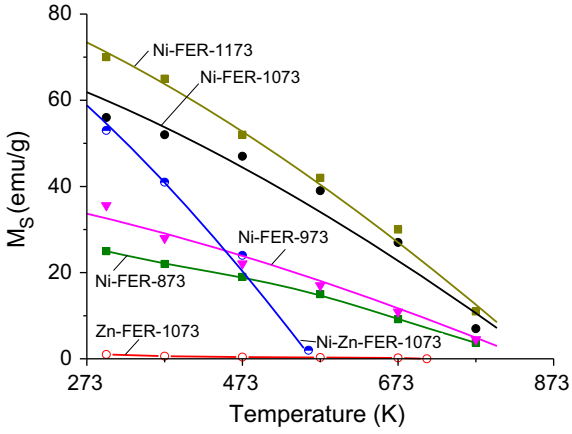

Fig. 5. Saturation magnetization as a function of temperature. Symbols represent experimental data. The solid lines represent Eq. (1).

(all values are in CGS) where the surface energy of the domain wall, ε_p, is defined as follows:

$$\varepsilon_p = \left(\frac{2k_B T_C K_1}{a}\right)^{0.5} \tag{3}$$

where k_B is the Boltzmann constant, T_c is the Curie temperature, a is the lattice parameter, and K_1 is the absolute value of magnetocrystalline anisotropy constant. The values of individual parameters are listed in Table 3.

The critical size of Ni ferrite of 41 nm is close to the domain size in Ni-FER-1073 sample. The difference is due to the fact that, for the calculation, we have used a simplified model, which does not take into consideration the shape of the particles and the interactions between them. In the single domain region, the coercivity decreases as the particle size is reduced, since the alignment of the

Table 2
Fitting parameters for the temperature dependence of M_s according to Eq. (1).

Sample	M_{s0} (emu/g)	B (K^{-b})	b (–)
Ni-FER-1173	89.6	4.0×10^{-5}	1.5
Ni-FER-1073	75.5	4.0×10^{-5}	1.5
Ni-FER-973	41.3	4.1×10^{-5}	1.5
Ni–Zn-FER-1073	88.9	7.5×10^{-5}	1.5

Table 3
Parameters used in estimation of critical grain size.

Parameter	Dimension	Ni-FER	Ni–Zn-FER	Reference
T_c	K	854	550	This study
a	cm	8.34×10^{-8}	8.40×10^{-8}	This study
M_{sp}	G	390	310	This study
K_1	erg/cm^3	7.0×10^4	1.5×10^4	[43,44]
ε_p	erg/cm^2	0.44	0.16	Eq. (3)
d_{cr}	nm	41	24	Eq. (2)

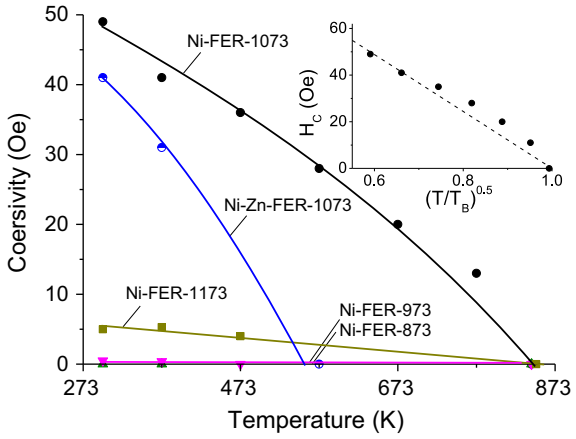

Fig. 6. Coercivity of samples as a function of temperature. Ni-FER-873, Ni-FER-973, Ni-FER-1073, and Ni-FER-1173. Symbols represent experimental data. The solid lines represent Eq. (4). Inset: coersivity of Ni-FER-1073 as a function of $(T/T_B)^{0.5}$.

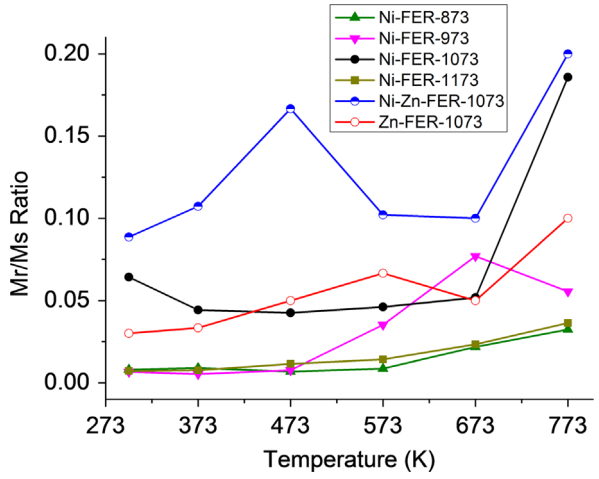

Fig. 7. M_r/M_s ratio as a function of temperature.

magnetic moments inside the domain is fully controlled by thermal energy, resulting in superparamagnetic behavior. The absence of hysteresis in the M–H loop (hysteresis loss below 0.4 kJ/m^3) demonstrates that Ni-FER-873 and Ni-FER-973 are superparamagnetic. The highest coercivity of 50 Oe was observed in Ni-FER-1073 (Fig. 6). This sample has the grain size close to transition size from single to multidomain region. Coercivity further decreases indicating multidomain nature of Ni-FER-1173 sample. Besides that low value of M_r/M_s ratio (below 0.2) also validates the existence of multidomains in Ni-FER-1173 (Fig. 7).

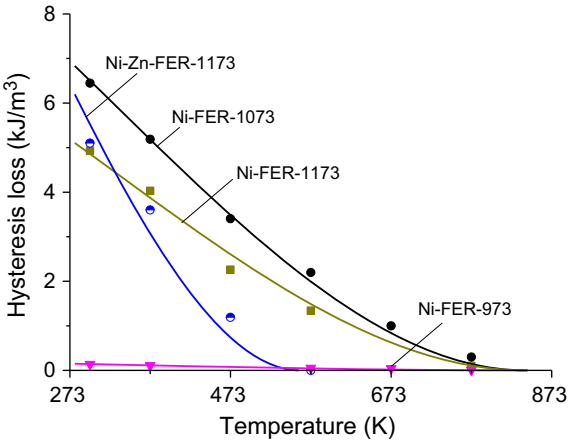

Fig. 8. Hysteresis losses of Ni-FER-873, Ni-FER-973, Ni-FER-1073, and Ni-FER-1173 as a function of temperature. Symbols represent experimental data. The solid lines represent Eq. (5).

In noninteracting ensembles of ferromagnetic nanoparticles, H_c decreases with an increase in temperature, the $H_c(T)$ dependence should obey the following relation [37]:

$$H_c = H_{c0}\left(1-\sqrt{\frac{T}{T_B}}\right) \tag{4}$$

where H_{c0} is the coercivity at $T=0$ K and T_B is the blocking temperature below which hysteresis appears. It can be seen from the inset of Fig. 6 that H_c decreases with the increase of temperature. There is a substantial deviation in linearity of temperature. The substantial deviation in linearity of H_c ($T^{0.5}$) for ferromagnetic Ni-FER-1073 (Fig. 6, inset) and Ni-FER-1173 (not shown) is an indication of the interparticle interactions.

As the grain size increases, the Curie temperature slightly increases from 849 to 859 K (Table 1). A similar trend was observed by Sepelak et al. for nanoscale high-energy-milled Ni ferrites [24]. These authors observed that Néel temperature (T_N) increases from 849 to 858 K with increasing annealing temperature from 1018 to 1198 K due to the cation reequilibration process. The increase in the T_N with sintering temperature has also been observed in nanostructured $MgFe_2O_4$ [38].

The hysteresis loss is an important factor when the performance of materials intended for RF heating is evaluated. The hysteresis loss, P (J/m^3), is proportional to the area between the two magnetization curves. It can be seen in Fig. 4 that the flux density increases rapidly in proportion to the field strength until it reaches 500 Oe then it increases more slowly and the latter part does not contribute much to the hysteresis losses. Therefore it is reasonable to assume that the hysteresis loss should be proportional to the product of H_c and M_s:

$$P = C_0 H_c M_s \tag{5}$$

where C_0 is a constant, which shows the ratio of the actual hysteresis loss and that in the case when the magnetization curves form a rectangle with edges of M_s and H_c. The temperature dependencies of M_s and H_c are expressed by Eqs. (1) and (4), respectively. The solid lines in Fig. 8 represent calculated values obtained by Eq. (5). It can be seen that a rather good agreement between the calculated and experimental data is observed in the whole temperature range for all Ni ferrite samples. The coefficient C_0 was obtained by the extrapolation method.

The Ni-FER-1073 has the highest hysteresis losses which also explain the highest specific heating rate of 1.6 K/s observed over this sample (Table 1). The specific heating rate of other ferrite samples decreases proportionally to the hysteresis loss. Therefore

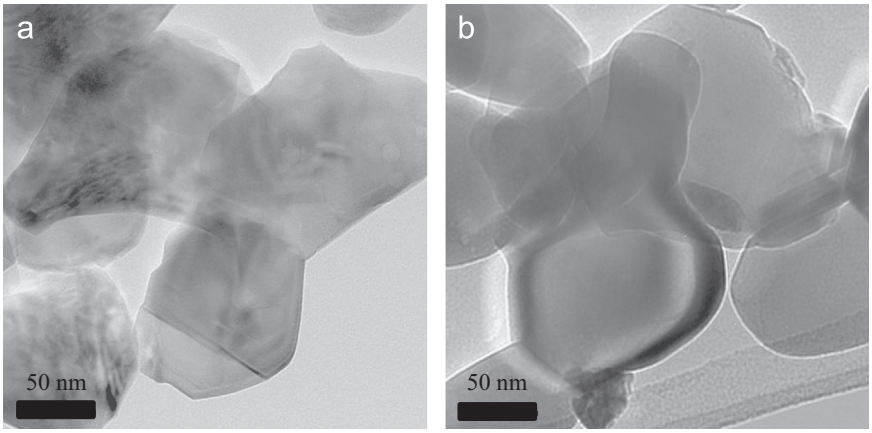

Fig. 9. TEM images of (a) Zn-FER-1073 and (b) Ni–Zn-FER-1073.

temperature dependencies of H_c and M_s can be used to predict specific heating rates at different temperatures.

In further experiments, the annealing temperature was fixed at 1073 K and effect of Zn addition has been studied.

3.3. *Effect of Zn addition on magnetic properties of ferrites*

XRD patterns of the Ni–Zn and Zn ferrites calcined at 1073 K are shown in Fig. 2e and f. The (311) interplanar spacing increases from 0.2516 to 0.2525 nm in Ni–Zn-FER-1073, because the Zn^{2+} atomic radius of 0.74 Å is slightly larger than that of the Ni^{2+} cation (0.70 Å). It can be seen that Zn addition reduces the magnetic attraction between individual nanoparticles and prevents their agglomeration during sintering. Therefore the specific surface area of Ni–Zn ferrite samples increases as compared to that in Ni ferrites. TEM image of Ni–Zn-FER-1073 is shown in Fig. 9a. The corresponding TEM images of Ni-FER-1073 and Zn-FER-1073 are shown in Figs. 3c and 9b, respectively. The $Ni_{0.5}Zn_{0.5}Fe_2O_4$ and Zn ferrite nanoparticles consist of irregular and oval polyhedrons with mean sizes between 50 and 100 nm. In this case, the particle size is bigger than the crystallite size obtained from the XRD analysis. Several "necks" between the two neighborhood particles are still observed which were formed during the sintering process [16].

The M_s of Ni–Zn-FER-1073 is smaller than those obtained for Ni-FER-1073 (Fig. 5). Kodama et al. [39] attributed the reduction in magnetization to the canted spin arrangements at the surface of the nanoparticles. In Ni–Zn-FER-1073, weakening of the A–B interactions is due to the effect of spin canting at the surface that dominates over the effect of site exchange of the cations. It could thus be presumed that the lower value of magnetization is a result of the weakening of the A–B interaction and pronounced surface spin disorder [40]. In the absence of the spin canting effect, or when its contribution could be neglected, much higher values of M_s were reported (Table 4).

As the temperature increases, M_s decreases (Fig. 5). The Bloch exponent b is equal to that observed in the Ni ferrites, while constant B is considerably larger (Table 2).

Fig. 6 shows a decrease in coercivity with addition of Zn that can be explained on the basis of magnetocrystalline anisotropy. Since the magnetocrystalline anisotropy constants of Ni-ferrite is larger than that of Zn-ferrite [40], replacing Ni^{2+} by the Zn^{2+} ions leads to a decrease in the value of coercivity as compared to that in Ni ferrite. The critical size estimated by Eq. (1) for Ni–Zn-FER-1073 is 24 nm (Table 2). This is in agreement with recent data by Li and Wang [41] who reported that monodispesed $Ni_{0.5}Zn_{0.5}Fe_2O_4$ particles in the 6–20 nm range were superparamagnetic. Thus, the chosen synthesis conditions allow to obtain Ni–Zn ferrites with the grain size in the transition from single to multidomain region, which is important to obtain the highest heating rate.

Table 4
Saturation magnetization of Ni–Zn ferrites prepared by different methods.

Composition	Method of processing	Sintering temperature (°C)	M_s (emu/g)	Reference
$Ni_{0.65}Zn_{0.35}Fe_2O_4$	Sol–gel	1373	80	[21]
$Ni_{0.5}Zn_{0.5}Fe_2O_4$	Ball milling	1373	75.9	[45]
$Ni_{0.65}Zn_{0.35}Fe_2O_4$	Citrate precursor	1473	73	[42]
$Ni_{0.5}Zn_{0.5}Fe_2O_4$	Ball milling	1073	66	[46]
$Ni_{0.5}Zn_{0.5}Fe_2O_4$	Co-precipitation	1623	63	[47]
$Ni_{0.5}Zn_{0.5}Fe_2O_4$	Sol–gel	1173	53	This study
$Ni_{0.5}Zn_{0.5}Fe_2O_4$	Hydrothermal	1573	41.6	[48]

The decrease in the Curie temperature with addition of Zn is clearly evident (Table 1). Zn^{2+} ions are known to occupy the tetrahedral (A) sites, Ni^{2+} ions have a preference for the octahedral (B) sites while the Fe^{3+} ions are distributed over both the sites. As the concentration of non-magnetic zinc ions on A sites increases, the Fe^{3+} ions migrate from tetrahedral A to octahedral B sites. The decrease in the magnetic ions at A site decreases the A–B interaction thereby decreasing the Curie temperature in the Ni–Zn ferrite. The value observed in the present work (558 K) is in close agreement with that reported by Verma et al. [42] for $Ni_{0.5}Zn_{0.5}Fe_2O_4$ ferrite prepared by the citrate precursor method.

Lower coercivity of $Ni_{0.5}Zn_{0.5}Fe_2O_4$ is favorable for RF heating as the same amount of heat can be generated at lower field intensity. The $Ni_{0.5}Zn_{0.5}Fe_2O_4$ exhibits relatively high heating rate of 1.4 K/s which is close to that of Ni-ZER-1073 (Table 1).

4. Conclusions

Nanocrystalline $NiFe_2O_4$ and $Ni_{0.5}Zn_{0.5}Fe_2O_4$ samples with moderate surface area of 17–35 m^2/g and coercivity below 50 Oe have been prepared by the sol–gel method. Influence of sintering temperature on the magnetic properties, hysteresis loss, and specific heating rate at 295 kHz has been studied. A method for estimation of the temperature dependence of specific heating rate from magnetization curves has been proposed. The critical sizes for $NiFe_2O_4$ and $Ni_{0.5}Zn_{0.5}Fe_2O_4$, corresponding to a transition to a multidomain region, were 41 and 24 nm, respectively. The highest saturation magnetization of 53 emu/g was observed over $Ni_{0.5}Zn_{0.5}Fe_2O_4$ sintered at 1073 K. This sample demonstrated a specific heating rate of 1.4 K/s. As the temperature increases, the

saturation magnetization decreases as $T^{1.5}$. The obtained materials can be employed in different applications where fast heating of the reaction medium is of importance.

Acknowledgments

The financial support from the Royal Academy of Engineering for research exchange with China and India—Major Award, the Science and Technology Planning Project of Hunan Province, China (2012WK3023) and the European Research Council (Project 279867, "RF-enhanced microprocessing for fine chemicals synthesis using catalysts supported on magnetic nanoparticles, RFMiFiCS"), is gratefully acknowledged. We thank Seagate Technology (Ireland) for their financial support to establish ANSIN (www.ansin.eu).

References

[1] R. Benrabaa, H. Boukhlouf, A. Löfberg, A. Rubbens, R.-N. Vannier, E. Bordes-Richard, A. Barama, Nickel ferrite spinel as catalyst precursor in the dry reforming of methane: synthesis, characterization and catalytic properties, Journal of Natural Gas Chemistry 21 (2012) 595–604.
[2] T.K. Houlding, E.V. Rebrov, Application of alternative energy forms in catalytic reactor engineering, Green Processing and Synthesis 1 (2012) 19–32.
[3] E.V. Rebrov, P. Gao, T.M.W.G.M. Verhoeven, J.C. Schouten, R. Kleismit, Z. Turgut, G. Kozlowski, Structural and magnetic properties of sol–gel $Co_{2x}Ni_{0.5-x}Zn_{0.5-x}Fe_2O_4$ thin films, Journal of Magnetism and Magnetic Materials 323 (2011) 723–729.
[4] P. Gao, E.V. Rebrov, T.M.W.G.M. Verhoeven, J.C. Schouten, R. Kleismit, G. Kozlowski, J. Cetnar, Z. Turgut, G. Subramanyam, Structural investigations and magnetic properties of sol–gel $Ni_{0.5}Zn_{0.5}Fe_2O_4$ thin films for microwave heating, Journal of Applied Physics 107 (2010) 044317.
[5] A. Ovenston, J.R. Walls, Generation of heat in a single catalyst pellet placed in an electromagnetic field for endothermic reforming of hydrocarbons, Journal of the Chemical Society Faraday Transactions 1: Physical Chemistry in Condensed Phases 79 (1983) 1073–1084.
[6] S.I. Al-Mayman, S.M. Al-Zahrani, Catalytic cracking of gas oils in electromagnetic fields: reactor design and performance, Fuel Processing Technology 80 (2003) 169–182.
[7] P. Duquenne, A. Deltour, G. Lacoste, Application of inductive heating to granular media: temperature distribution in a granular bed, International Journal of Heat and Mass Transfer 36 (1993) 2473–2477.
[8] T.K. Houlding, K. Tchabanenko, M.T. Rahman, E.V. Rebrov, Direct amide formation using radiofrequency heating, Organic and Biomolecular Chemistry 11 (2013) 4171–4177.
[9] C.N. Chinnasamy, A. Narayanasamy, N. Ponpandian, K. Chattopadhyay, K. Shinoda, B. Jeyadevan, K. Tohji, K. Nakatsuka, T. Furubayashi, I. Nakatani, Mixed spinel structure in nanocrystalline $NiFe_2O_4$, Physical Review B 63 (2001) 184108.
[10] L.D. Tung, V. Kolesnichenko, G. Caruntu, D. Caruntu, Y. Remond, V.O. Golub, C. J. O'Connor, L. Spinu, Annealing effects on the magnetic properties of nanocrystalline zinc ferrite, Physica B: Condensed Matter 319 (2002) 116–121.
[11] K. Maaz, S. Karim, A. Mumtaz, S.K. Hasanain, J. Liu, J.L. Duan, Synthesis and magnetic characterization of nickel ferrite nanoparticles prepared by co-precipitation route, Journal of Magnetism and Magnetic Materials 321 (2009) 1838–1842.
[12] M. George, A. Mary John, S.S. Nair, P.A. Joy, M.R. Anantharaman, Finite size effects on the structural and magnetic properties of sol–gel synthesized $NiFe_2O_4$ powders, Journal of Magnetism and Magnetic Materials 302 (2006) 190–195.
[13] V.K. Sankaranarayanan, C. Sreekumar, Precursor synthesis and microwave processing of nickel ferrite nanoparticles, Current Applied Physics 3 (2003) 205–208.
[14] M. Jalaly, M.H. Enayati, P. Kameli, F. Karimzadeh, Effect of composition on structural and magnetic properties of nanocrystalline ball milled $Ni_{1-x}Zn_xFe_2O_4$ ferrite, Physica B: Condensed Matter 405 (2010) 507–512.
[15] M.A.A. Elmasry, A. Gaber, E.M.H. Khater, Preparation of nickel ferrite using the aerosolization technique: Part I: aerosolization behaviour of individual raw material solutions, Powder Technology 90 (1997) 161–164.
[16] A. Dias, R.L. Moreira, N.D.S. Mohallem, Sintering studies of hydrothermal NiZn ferrites, Journal of Physics and Chemistry of Solids 58 (1997) 543–549.
[17] A. Azizi, S.K. Sadrnezhaad, Effects of annealing on phase evolution, microstructure and magnetic properties of mechanically synthesized nickel-ferrite, Ceramics International 36 (2010) 2241–2245.
[18] W. Yan, L. Wang, Z. Xia, M. Cheng, Q. Li, Y. Zhang, Effect of $PbO–SiO_2$ and $PbO–B_2O_3$ flux systems on the crystalline and magnetic properties of $Ni_{0.5}Zn_{0.5}Fe_2O_4$ ferrite prepared from the mixed powders, Materials Research Bulletin 42 (2007) 1468–1472.
[19] N.D.S. Mohallem, L.M. Seara, Magnetic nanocomposite thin films of $NiFe_2O_4/SiO_2$ prepared by sol–gel process, Applied Surface Science 214 (2003) 143–150.
[20] P.S.A. Kumar, J.J. Shrotri, S.D. Kulkarni, C.E. Deshpande, S.K. Date, Low temperature synthesis of $Ni_{0.8}Zn_{0.2}Fe_2O_4$ powder and its characterization, Materials Letters 27 (1996) 293–296.
[21] A.M. Kumar, M.C. Varma, C.L. Dube, K.H. Rao, S.C. Kashyap, Development of Ni–Zn nanoferrite core material with improved saturation magnetization and DC resistivity, Journal of Magnetism and Magnetic Materials 320 (2008) 1995–2000.
[22] S. Zahi, A.R. Daud, M. Hashim, A comparative study of nickel–zinc ferrites by sol–gel route and solid-state reaction, Materials Chemistry and Physics 106 (2007) 452–456.
[23] C.N. Chinnasamy, A. Narayanasamy, N. Ponpandian, K. Chattopadhyay, H. Guérault, J.-M. Greneche, Magnetic properties of nanostructured ferrimagnetic zinc ferrite, Journal of Physics: Condensed Matter 12 (2000) 7795.
[24] V. Šepelák, U. Steinike, D.C. Uecker, S. Wißmann, K.D. Becker, Structural disorder in mechanosynthesized zinc ferrite, Journal of Solid State Chemistry 135 (1998) 52–58.
[25] H.H. Hamdeh, J.C. Ho, S.A. Oliver, R.J. Willey, G. Oliveri, G. Busca, Magnetic properties of partially-inverted zinc ferrite aerogel powders, Journal of Applied Physics 81 (1997) 1851–1857.
[26] T. Sato, K. Haneda, M. Seki, T. Iijima, Morphology and magnetic properties of ultrafine $ZnFe_2O_4$ particles, Applied Physics A 50 (1990) 13–16.
[27] N. Ponpandian, A. Narayanasamy, C.N. Chinnasamy, N. Sivakumar, J.-M. Greneche, K. Chattopadhyay, K. Shinoda, B. Jeyadevan, K. Tohji, Neel temperature enhancement in nanostructured nickel zinc ferrite, Applied Physics Letters 86 (2005) 192510.
[28] E.E. Sileo, R. Rotelo, S.E. Jacobo, Nickel zinc ferrites prepared by the citrate precursor method, Physica B: Condensed Matter 320 (2002) 257–260.
[29] A.L. Patterson, The Scherrer formula for X-ray particle size determination, Physical Review 56 (1939) 978–982.
[30] M.A. Gabal, Effect of Mg substitution on the magnetic properties of NiCuZn ferrite nanoparticles prepared through a novel method using egg white, Journal of Magnetism and Magnetic Materials 321 (2009) 3144–3148.
[31] J.F. Löffler, H.-B. Braun, W. Wagner, Magnetic correlations in nanostructured ferromagnets, Physical Review Letters 85 (2000) 1990–1993.
[32] D. Zhang, K.J. Klabunde, C.M. Sorensen, G.C. Hadjipanayis, Magnetization temperature dependence in iron nanoparticles, Physical Review B 58 (1998) 14167–14170.
[33] D.L. Mills, A.A. Maradudin, Some thermodynamic properties of a semi-infinite Heisenberg ferromagnet, Journal of Physics and Chemistry of Solids 28 (1967) 1855–1874.
[34] P.V. Hendriksen, S. Linderoth, P.A. Lindgård, Finite-size modifications of the magnetic properties of clusters, Physical Review B 48 (1993) 7259–7273.
[35] J.P. Chen, C.M. Sorensen, K.J. Klabunde, G.C. Hadjipanayis, E. Devlin, A. Kostikas, Size-dependent magnetic properties of MnFe2O4 fine particles synthesized by coprecipitation, Physical Review B 54 (1996) 9288–9296.
[36] I.Z. Rahman, T.T. Ahmed, A study on Cu substituted chemically processed Ni–Zn–Cu ferrites, Journal of Magnetism and Magnetic Materials 290–291 (2) (2005) 1576–1579.
[37] E.H. Frei, S. Shtrikman, D. Treves, Critical size and nucleation field of ideal ferromagnetic particles, Physical Review 106 (1957) 446–455.
[38] V. Šepelák, D. Schultze, F. Krumeich, U. Steinike, K.D. Becker, Mechanically induced cation redistribution in magnesium ferrite and its thermal stability, Solid State Ionics 141–142 (2001) 677–682.
[39] R.H. Kodama, A.E. Berkowitz, J.E.J. McNiff, S. Foner, Surface spin disorder in $NiFe_2O_4$ nanoparticles, Physical Review Letters 77 (1996) 394–397.
[40] M. Younas, M. Atif, M. Nadeem, M. Siddique, M. Idrees, R. Grossinger, Colossal resistivity with diminished tangent loss in Zn–Ni ferrite nanoparticles, Journal of Physics D: Applied Physics 44 (2011) 345402.
[41] X. Li, G. Wang, Low-temperature synthesis and growth of superparamagnetic $Zn_{0.5}Ni_{0.5}Fe_2O_4$ nanosized particles, Journal of Magnetism and Magnetic Materials 321 (2009) 1276–1279.
[42] A. Verma, T.C. Goel, R.G. Mendiratta, P. Kishan, Magnetic properties of nickel–zinc ferrites prepared by the citrate precursor method, Journal of Magnetism and Magnetic Materials 208 (2000) 13–19.
[43] C. Sujatha, K. Venugopal Reddy, K. Sowri Babu, A. Ramachandra Reddy, K.H. Rao, Effect of sintering temperature on electromagnetic properties of NiCuZn ferrite, Ceramics International 39 (2013) 3077–3086.
[44] C. Caizer, M. Stefanescu, Nanocrystallite size effect on σ_s and H_c in nanoparticle assemblies, Physica B: Condensed Matter 327 (2003) 129–134.
[45] E. Rezlescu, L. Sachelarie, P.D. Popa, N. Rezlescu, Effect of substitution of divalent ions on the electrical and magnetic properties of Ni–Zn–Me ferrites, IEEE Transactions on Magnetics 36 (2000) 3962–3967.
[46] J.S. Jiang, L. Gao, X.L. Yang, J.K. Guo, H.L. Shen, Nanocrystalline NiZn ferrite synthesized by high energy ball milling, Journal of Materials Science Letters 18 (1999) 1781–1783.
[47] A.S. Albuquerque, J.D. Ardisson, W.A.A. Macedo, M.C.M. Alves, Nanosized powders of NiZn ferrite: synthesis, structure, and magnetism, Journal of Applied Physics 87 (2000) 4352–4357.
[48] S.L. Pereira, H.D. Pfannes, A.A. Mendes, F.M. Ho, L.C.B. Miranda Pinto, M.A. Chincaro, A comparative study of NiZn ferrites modified by the addition of cobalt, Journal of Materials Research 2 (1999) 231–234.